Ziesch, J., Aruffo, C. M., Tanner, D. C., Beilecke, T., Dance, T., Henk, A., Weber, B., Tenthorey, E., Lippmann, A., Krawczyk, C. M. (2017): Geological structure and kinematics of normal faults in the Otway Basin, Australia, based on quantitative analysis of 3-D seismic reflection data. - *Basin Research*, *29*, 2, pp. 129—148.

DOI: http://doi.org/10.1111/bre.12146

according to Basin Research (2017), 29, 129-148, doi: 10.1111/bre.12146

Geological structure and kinematics of normal faults in the Otway Basin, Australia, based on quantitative analysis of 3-D seismic reflection data

Jennifer Ziesch: *Leibniz Institute for Applied Geophysics*, Stilleweg 2, 30655 Hannover, Germany, e-mail: Jennifer.Ziesch@liag-hannover.de
Chiara M. Aruffo: *Technical University Darmstadt*—Institut for Applied Geosciences, Schnittspahnstrasse 9, Darmstadt 64287, Germany
David C. Tanner : *Leibniz Institute for Applied Geophysics*, Stilleweg 2, 30655 Hannover, Germany
Thies Beilecke: *Leibniz Institute for Applied Geophysics*, Stilleweg 2, 30655 Hannover, Germany
Tess Dance: a) *CRC for Greenhouse Gas Technologies (CO2CRC) b)CSIRO Petroleum Resources*, Kensington, WA 6151, Australia.
Andreas Henk: *Technical University Darmstadt*—Institut for Applied Geosciences, Schnittspahnstrasse 9, Darmstadt 64287, Germany
Bastian Weber: *Technical University Darmstadt*—Institut for Applied Geosciences, Schnittspahnstrasse 9, Darmstadt 64287, Germany
Eric Tenthorey: *Geoscience Australia*, GPO Box 378 Canberra ACT 2601 Australia
Andrea Lippmann: *TEEC Geophysics*, Burgwedelerstr. 89, 30916 Isernhagen, Germany
Charlotte M. Krawczyk: *Leibniz Institute for Applied Geophysics*, Stilleweg 2, 30655 Hannover, Germany; now at *GFZ Potsdam*, Germany.

Abstract

The Otway Basin in the south of Victoria, Australia underwent three phases of deformation during breakup of the southern Australian margin. We assess the geometry and kinematics of faulting in the basin by analysing a 3-D reflection seismic volume. Eight stratigraphic horizons and 24 SW-dipping normal faults as well as subordinate antithetic faults were interpreted. This resulted in a high-resolution geological 3-D model (ca. 8 km × 7 km × 4 km depth) that we present as a supplementary 3-D PDF. We identified hard- and soft-linking fault connections over the entire area, such as antithetic faults and relay ramps, respectively. Most major faults were continuously active from Early to Late Cretaceous, with two faults in the northern part of the study area active until at least the Oligocene. Allan maps of faults show tectonic activity continuously waned over this time period. Isopach maps of stratigraphic volumes quantify the amount of syn-sedimentary movement that is characteristic of passive margins, such as the Otway Basin. We show that the faults possess strong corrugations (with amplitudes above the seismic resolution), which we illustrated by novel techniques, such as cylindricity and curvature. We argue that the corrugations are produced by sutures between sub-vertical fault segments and this morphology was maintained during fault growth. Thus they can be used to indicate the kinematics vector of the fault movement. This evidences, together with left-stepping relay ramps, that 40% of the faults had a small component (up to 25°) of dextral oblique slip as well as normal (dip-slip) movement.

1 Introduction

Tectonic communication between reservoir and surface is one of the most important issues when analysing reservoir integrity. Therefore particular emphasis must be given to imaging and characterisation of geological faults during the exploration stage. Fault dynamics must be thoroughly assessed since they offer first-order linkage and thus maybe possible pathways. This requires qualitative and quantitative description of the tectonic deformation, such as has been addressed in several fault analysis studies in many different settings during the last 35 years (e.g., Taylor & Hayes, 1980; Needham et al., 1996a; Contreras et al., 2000; Dawers & Underhill, 2000; McLeod et al., 2000; Morley, 2002; Kley et al., 2005; Tvedt et al., 2013).

In regions of extensional tectonics, the knowledge of the fault geometry and kinematics plays a key role in understanding the nature of the tectonic movement (e.g., White et al. 1986). Certain aspects of faults have been analysed, such as their growth and linkage (e.g., Peacock and Sanderson, 1991; Cartwright et al., 1995; Nicol et al., 2005) and interconnected networks (e.g., Nixon et al., 2014). But especially analysis of fault morphology, for instance derived from 3-D seismic interpretation, are rare (e.g., Needham et al., 1996b; Lohr et al., 2008). Much more work has been carried out on small-scale outcrops of faults, especially where the host material can be sequentially removed or examined in three-dimensions (e.g., Fossen & Hesthammer 1997; Brandes & Tanner 2012; Awdal et al., 2014). Fault juxtapostion (Allan) maps and isochore maps of fault throw are often used to determine fault sealing (e.g., Lindsay et al. 1993; Yielding et al. 1997), but more importantly they can be used to postulate fault growth and kinematics (e,g. Walsh & Watterson, 1989; Lohr et al., 2008). Corrugations on the fault surfaces have become more important, because they may contain information about fault kinematics, which are otherwise unobtainable (Hancock & Barka 1987; Needham et al., 1996b).

Our project, named PROTECT, stands for ‘Prediction Of deformation To Ensure Carbon Traps’ (Krawczyk et al., 2015). Our working area is the CO2CRC Otway project site (Jenkins et al., 2011; Cook, 2014) in south-western Victoria, Australia (Fig. 1). Previous studies at the CO2CRC Otway site have focused on geological site characterisation (e.g., Dance, 2013), seismic measurements (for an overview see Gurevich et al., 2014), including time-lapse surveying (e.g., Urosevic et al., 2011; Pevzner et al., 2013), and geomechanical analysis (e.g., van Ruth et al., 2007; Vidal-Gilbert et al., 2010; Aruffo et al., 2014).

The focus of this paper is a high-resolution geological and structural analysis of 3-D seismics of the immediate area around the CO2CRC Otway site. In particular using juxtaposition (Allan) maps of faults and stratigraphic thickness maps, we analyse the contacts between faults, the relationship between sedimentation and faulting, and the temporal activity of faults. This paper also aims to provide novel techniques to characterise and identify the kinematics of normal faults in order to understand the formation of these faults within the Otway Basin. An analysis of fault corrugations (by analysing fault surface curvature and cylindricity) characterises and identifies the kinematics of normal faults and their formation within this area of the Otway Basin. Our aim is to understand the structure, geometry and tectonic evolution of the area, between the reservoir at 1800 m depth and the highest, still seismically-visible structures at ca. 400 m depth.

2 Geological setting

2.1 Tectonics of the Otway Basin

The Otway Basin is a NW-striking passive margin rift basin (Figs. 1 and 2) that formed during Gondwana break-up of Antarctic-Australian separation (Williamson et al., 1990). Its geodynamic evolution can be broadly divided into three phases of deformation (Norvick & Smith, 2001).

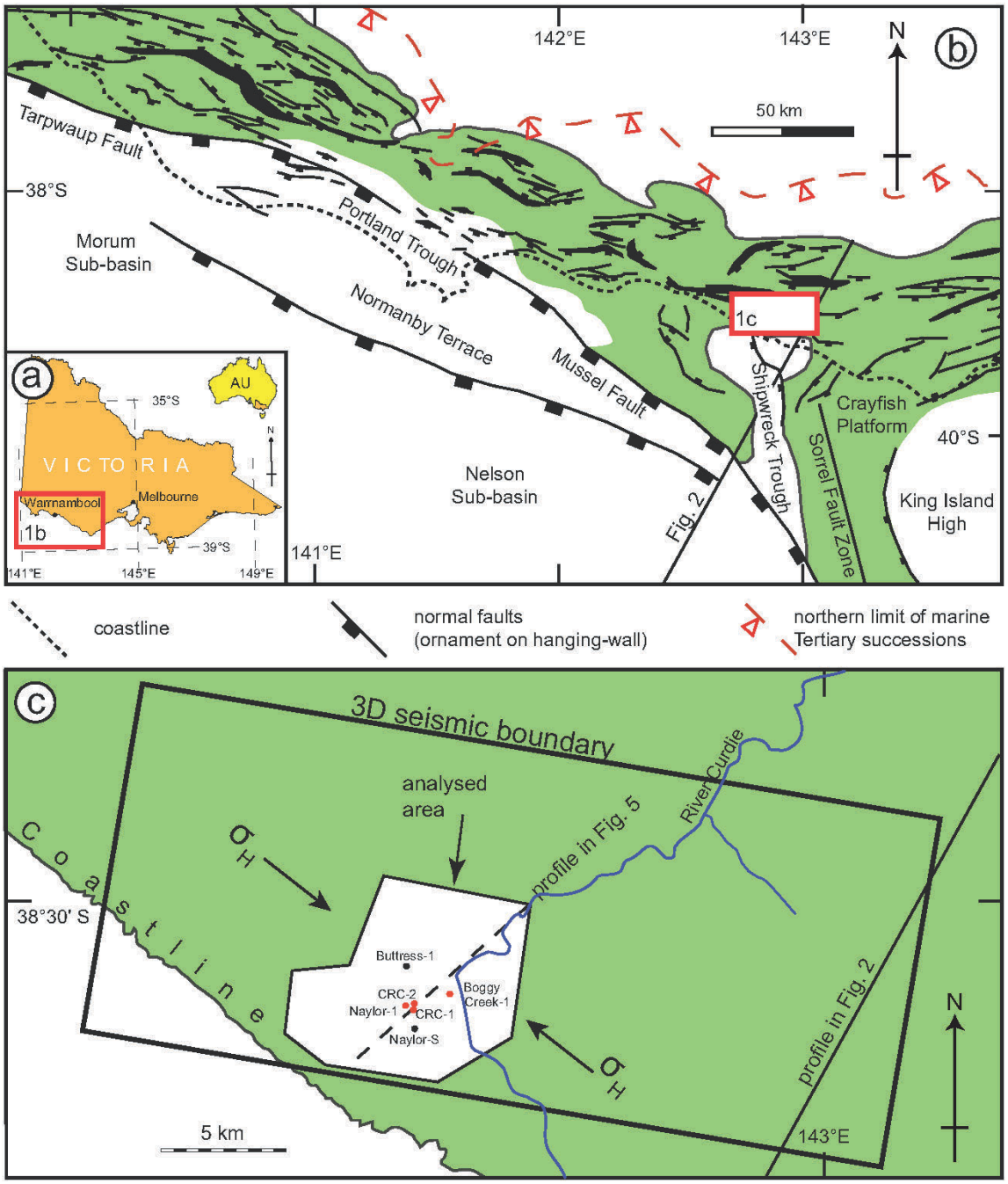

Figure 1: Location map. a) Map of the state of Victoria in Australia. Box marks area shown in b). b) Map showing the major normal faults in the Otway Basin and northern limit of marine Tertiary successions (Cretaceous sediments marked in green, compiled from Alley & Lindsay (1995); Moore et al. (2000); Perincek & Cockshell (1995); Douglas & Ferguson (1988). The location of the seismic transect in Fig. 2 is also shown. Red box marks area shown in c). c) Close-up of the analysed area, showing extent of the 3-D seismic dataset, important borehole locations, and the line of the profiles in Figs. 2 and 5. Boreholes marked red contained checkshot data that was used for the time-depth conversion. The Sorrel Fault zone is the boundary between the western and eastern Otway Basin.

The first deformation phase (Late Jurassic – Early Cretaceous) was characterised by rifting due to N–S extension (Cooper & Hill, 1997). The western Otway Basin is separated from the eastern part by the Sorrel Fault zone (Finlayson et al., 1996; Cooper & Hill, 1997; Miller et al., 2002, Fig. 1). In the western Otway Basin this caused

W–E or NW–SE striking normal faults (Miller et al., 2002). In some areas the W–E striking faults have a dextral strike-slip component (Perincek & Cockshell, 1995). In contrast, the eastern Otway Basin is dominated by NE–SW striking normal faults and subordinated N-trending faults with a sinistral strike-slip component. Rifting was followed by widespread thermal subsidence during the Aptian–Albian (Bryan et al., 1997). The second phase of deformation was compressional causing uplift and fault inversion in the mid-late Cretaceous (Norvick & Smith, 2001) and gave rise to the basin-wide Otway Unconformity (late Albian, 100 Ma). After a 6.5 Ma hiatus, the third deformation phase of NE–SW extension and rift-related subsidence began in the Turonian. During the third phase, fast continental spreading began in the Southern Ocean during the Lutetian (44 Ma), which lead to rapid thermal subsidence and marine transgression. In this phase the first oceanic crust was formed off the Otway Basin, which propagated southwards towards offshore west Tasmania. During the Miocene, in Otway, Gippsland and interior Australia, inversion began again, causing reverse faulting and folding (Norvick & Smith, 2001).

In the present-day tectonic setting, recent studies indicate the presence of a normal faulting stress regime in which $\sigma_v = \sigma_1$ and $\sigma_{Hmin} = \sigma_3$. The maximum horizontal stress orientation (σ_{Hmax}) has been inferred from borehole breakouts at the CRC-1 well (Fig. 1) to be N142 ± 5°E (van Ruth et al., 2007), a value that is consistent with the regional orientation NW–SE of σ_{Hmax} in the onshore Otway Basin (Hillis & Reynolds, 2000). In the CRC-1 well, the magnitude of σ_{Hmax} is comparable to that derived from the inversion of borehole sonic data (Bérard et al., 2008) with a gradient of 18.75 MPa km^{-1}. Interpretation of extended leak-off tests (van Ruth et al., 2007) led to the determination of the magnitude of minimum horizontal stress (σ_{Hmin}) with an average gradient of 14.62 MPa km^{-1}. The average vertical stress gradient is about 23.3 MPa km^{-1} (Vidal- Gilbert et al., 2010).

2.2 Stratigraphy

The strata of the Otway Basin can be divided into five unconformity-bound successions (Tupper et al., 1993): the Otway, Sherbrook, Wangerrip, Nirranda and Heytesbury Groups (Fig. 2, Perincek & Cockshell, 1995). The Otway Group is a succession of fluvio-lacustrine sediments, up to 8000 m thick that accumulated in graben and half-graben structures during the first rifting event (Late Jurassic – Early Cretaceous). It also contains large amounts of volcaniclastic material derived from the east (Kopsen & Scholefield, 1990; Tupper et al., 1993).

The Sherbrook Group unconformably overlies the Otway Group and consists of a succession of sand- and mudstones, up to 5000 m thick that accumulated during the third deformation phase in deltaic and restricted marine settings (Fig. 2). The Waarre Fm. of this group is the target reservoir for CO2 storage (Fig. 3). These sandstones are overlain by thick carbonaceous mudstones of the Belfast Mst. that forms a regional seal across most of the Otway Basin (Jones et al., 2000). The Paaratte Formation represents a deltaic depositional system that broadly prograded across facies of the Belfast Mst., while onshore it passes laterally into the more proximal deltaic facies of the Timboon Sst. (Fig. 3).

The Wangerrip Group represents the beginning of passive margin sedimentation after rifting ceased (Fig. 2). It unconformably overlies rocks of the Sherbrook Group and consists of up to 700 m of sandstones and mudstones. A thin basal unit, the Massacre Shale, passes upwards into the argillaceous sandstones of the Pebble Point Formation (Fig. 3, Tupper et al., 1993). The Pebble Point Fm. is in turn overlain by fine clastics of the Pember Mst. (Fig. 3), which also has a good potential as a regional seal. The Dilwyn Fm. comprises sand- and mudstone deposited in a range of marine and deltaic environments.

A major unconformity marks the beginning of rapid spreading in the Southern Ocean (Norvick & Smith, 2001) and separates the Nirranda Group from lower groups (Fig. 2). The basal Mepunga Fm. of the Nirranda Group consists of interbedded sandstone and mudstone deposited in proximal- to distal marine environments (Fig. 3).

Continued transgression created an open marine setting in which the fine-grained facies of the Narrawaturk Marl were deposited (Lavin, 1998). Fully marine conditions returned in the early Miocene with the deposition of calcareous mudstone, marls and sandy limestone of the Heytesbury Group. During the Pliocene, the Otway Basin underwent phases of inversion followed by deposition of fluvial sands, which continues up to present day (Norvick & Smith, 2001).

The study area is part of the western Otway Basin. The strata imaged in the seismic all belong to the third deformation phase. However, the faults that were analysed all formed during the first phase of deformation and were still active during the third phase.

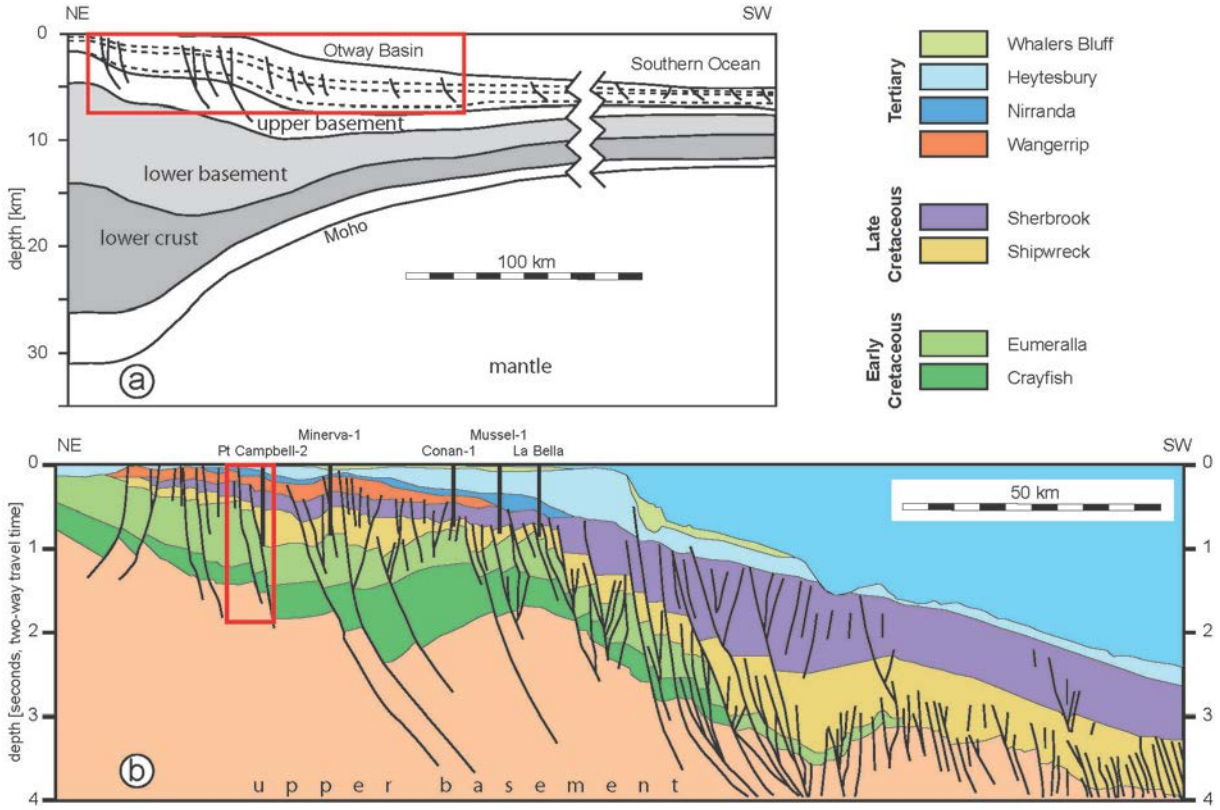

Figure 2: Large scale seismic cross-sections of the Otway Basin. Profile location is shown in Fig. 1. a) Crustal cross-section based on a 2D reflection seismic profile (Finlayson et al., 1998). Red box is the position of detailed structure given in b). Sedimentary units are denoted by dashed lines. b) Interpretation of seismic section through the Otway Basin, colour-coded for main stratigraphic groups (Blevin & Cathro, 2008). Red box denotes extent of the 3-D seismic dataset interpreted in this work.

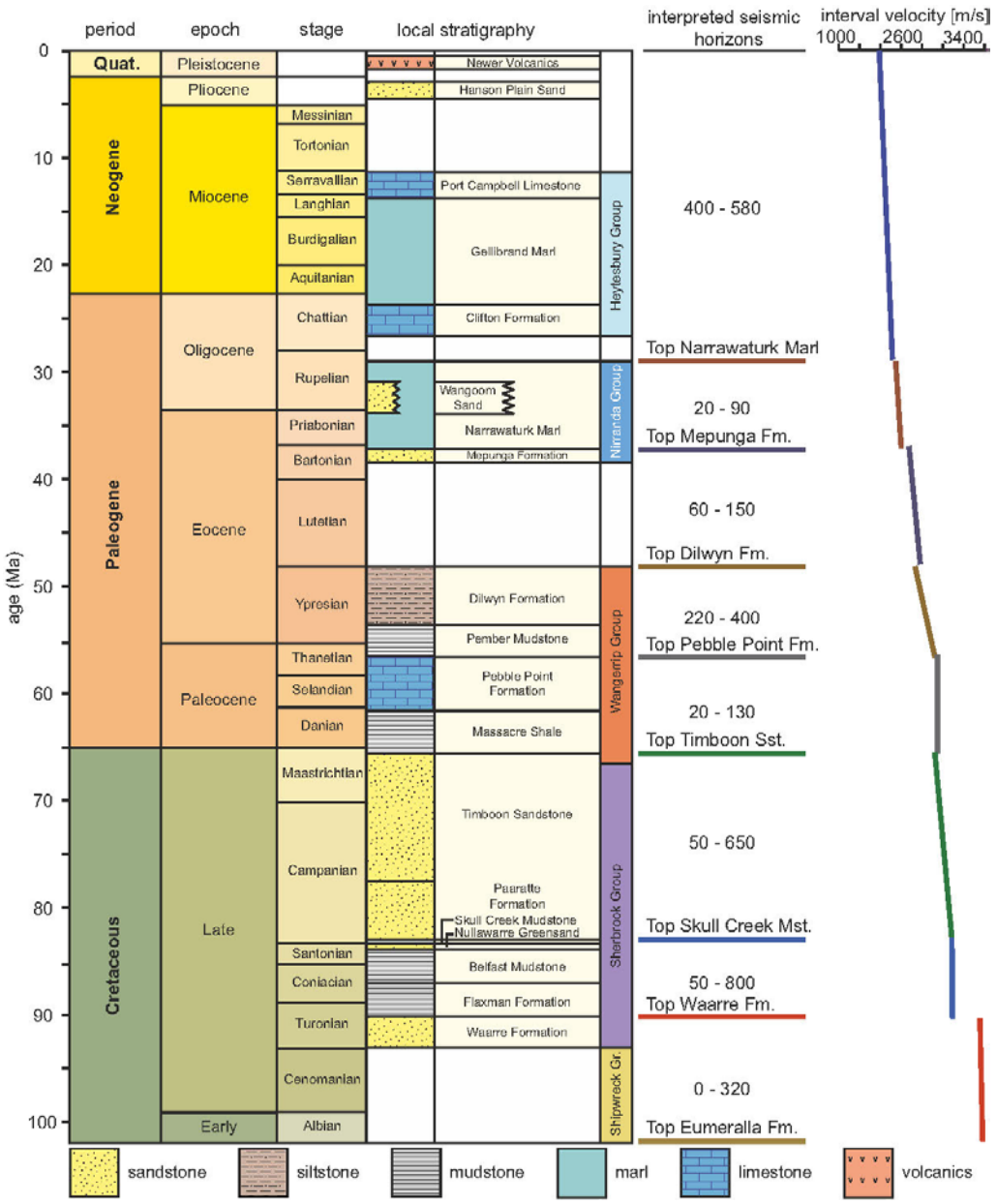

Figure 3: Detailed stratigraphy of the analysed area, modified after Perincek & Cockshell (1995). The key horizons picked in the 3-D seismic dataset are shown (colours as in the supplementary 3-D PDF), as are the ranges of thicknesses between the horizons (see Fig. 9 for detailed isopach maps). The graph shows the calculated interval velocities that were taken from 9 wells for the time-depth conversion.

3 Reflection seismic data base

We used a 3-D reflection seismic data cube (referred to as the Nirranda-Heytesbury 3-D survey) for seismic interpretation. It is a combination of three different surveys: the OGF93A, the ONH01, and the Curdie Vale 3-D (OCV00) surveys. This seismic volume is 32.3 km x 14.35 km x 4100 ms two-way traveltime (TWT) with a 24-fold bin size of 20 m by 20 m (Fig. 1). The data were acquired and processed in 2000 (CGG Australia Pty. Ltd., 2000). The signal frequency range used was 5–90 Hz, and the recorded offset range 28 m to 2280 m. 3-D poststack finite-difference time migration was used for imaging.

Most of the volume horizons and fault zones are well imaged. Since the target depth of the data acquisition geometry was the Waarre and Belfast Fms. (≈ 1.6 km depth), the uppermost 400 m of the dataset are less well-imaged, compared to the rest of the volume. We used SEG standard polarity for interpretation, i.e., negative impedance contrast is shown as a trough.

To determine a robust velocity model for time-depth conversion we used stratigraphic information (eight horizons) from the CRC-1 borehole (Fig. 1). For this purpose we determined the interval velocity at the tops of the individual formations and the velocity gradient within the respective formations. We relied on 9 wells in the larger volume to provide quality control for the depth conversion. On average, the depth error was 0.6% of formation depth in the wells.

4 Methods

4.1 3-D Seismic interpretation

The 3-D seismic data cube was interpreted in the time domain. For this study we focused on a smaller area around the injection well (ca. 8 km x 7 km; Fig. 1). Eight horizons were interpreted from the base of the reservoir formation (Waarre Fm.), which corresponds to the Top Eumeralla Fm., up to the highest seismically-visible horizon (Narrawaturk Fm.). Therefore, the stratigraphic units covered by the interpretation range from Early Cretaceous to Late Eocene (Fig. 3). Timboon Sst. and Paaratte Fm. were considered as a single formation, as well as Skull Creek Mst. and Belfast Fm. Formation tops from six wells in the subvolume constrained the seismic interpretation (Fig. 1). For our structural analysis we accurately picked surface morphologies of both stratigraphic horizons and faults.

One of the aims of the seismic interpretation was to accurately map the morphology of fault surfaces. Therefore, we used so-called random-lines perpendicular to the strike of the faults, in addition to the use of inlines and crosslines. For the faults we chose an interpretation spacing of 40–60 m. During the interpretation, seismic volume attributes, such as coherence, ant-tracking, variance, and instantaneous phase were invaluable. Using the 3-D-coherency and curvature processing (Lippmann et al., 2013) we were able to identify faults better. After depth conversion, we exported the interpreted stratigraphic horizons and faults as ASCII point sets for subsequent modelling work (Fig. 4a).

4.2 Surface modelling

The 3-D geological model was created with a meshing software (GOCAD®; Paradigm Ltd., 2009). The point-sets of the seismic interpretation were used as the basis for the triangulation of surfaces (Fig. 4b). Fault surfaces were created by direct tessellation of the originally-interpreted points. Only extremely diverging points were deleted. To gain the best compromise between spatial resolution and software limitation for the surfaces of the stratigraphic horizons we aimed for a triangle edge-length of 75 m. To build a consistent structural model we used a 'Structural Modelling' workflow. This consists of three steps:

1. Creation of a surface using the point-set of an interpreted horizon.
2. Creation of an intersection between fault surface and horizon surface. New points within the horizon surface were generated along the line of intersection.
3. Modelling of the vertical displacement, in which the original point-set were used as control points (Mallet, 2002). This means that during the generation of the fault/horizon intersections the horizon

surface was kept as close as possible to the original point-set. The horizon surface was opened along the fault surface (see Fig. 4b).

Due to artificial, interpretation-related roughness of the stratigraphic horizons, it was necessary to interpolate the surfaces. To ensure that the individual interpolated surfaces were still representative of the original point-sets, control points were used during the interpolation process (Mallet, 1992, 2002). By using control points the resulting surface had a minimal vertical difference to the original point-sets. Isopach maps of the stratigraphic units were generated and the isopach data were saved as attributes to the basal horizon.

We created a 3-D pdf (supplementary 3-D PDF) to give the readers the opportunity to examine the detailed geometry of the 3-D model themselves. All stratigraphic horizons and faults can be displayed in map or oblique view. The viewer also has the capability to create custom 2-D sections along X, Y, or Z axes through the 3-D model.

4.3 Structural analysis

The structural analysis was carried out with a kinematic modelling software (3DMove™; Midland Valley Exploration Ltd., 2013). The triangulated surfaces were used directly as input and were displayed using different attributes (Fig. 4c). We used the following tools in the software for structural analysis:

1. Allan mapper. This tool is used to view the juxtaposition of strata on the fault plane (Allan, 1989). It is used to measure the heave/throw/slip between the fault's hanging-wall and footwall cut-offs (or Allan lines). The results can be depicted as strike length/depth diagrams (termed in this work as Allan map). This allows us to determine the timing of faulting, fault growth and evolution of relay ramps. The Allan map can also be used to calculate 'throw-depth' plots.
2. Curvature Analysis. This tool is used to measure the curvature of fault surfaces. It gives a measure of the rate of change of angle across a surface and describes the fault morphology as the deviation of the triangulated surface from different plane. The calculation of the simple curvature is weighed to account for the surface areas of the triangles. A value for simple curvature is produced from the divergence of the normals of the triangles that surround a vertex, relative to the average normal (Midland Valley Exploration Ltd., 2013). Lower values show the tendency towards a flat plane and higher values show higher curvature. We use the curvature analysis to determine the amplitude of corrugation of the fault surface.
3. Cylindrical Analysis. This tool measures how well a triangulated surface fits a cylindrical surface. The smallest eigenvector is the fold axis of the folded surface, which here is referred to as the long axis of cylindricity. The orientation of a triangle's normal is compared to the orientation of the average cylindrical vector (parallel to fault corrugation, Lohr et al., 2008).
4. Orientation analysis of triangulated fault surfaces. We used this tool to create stereographic projections of the poles of all triangles of the fault surface.

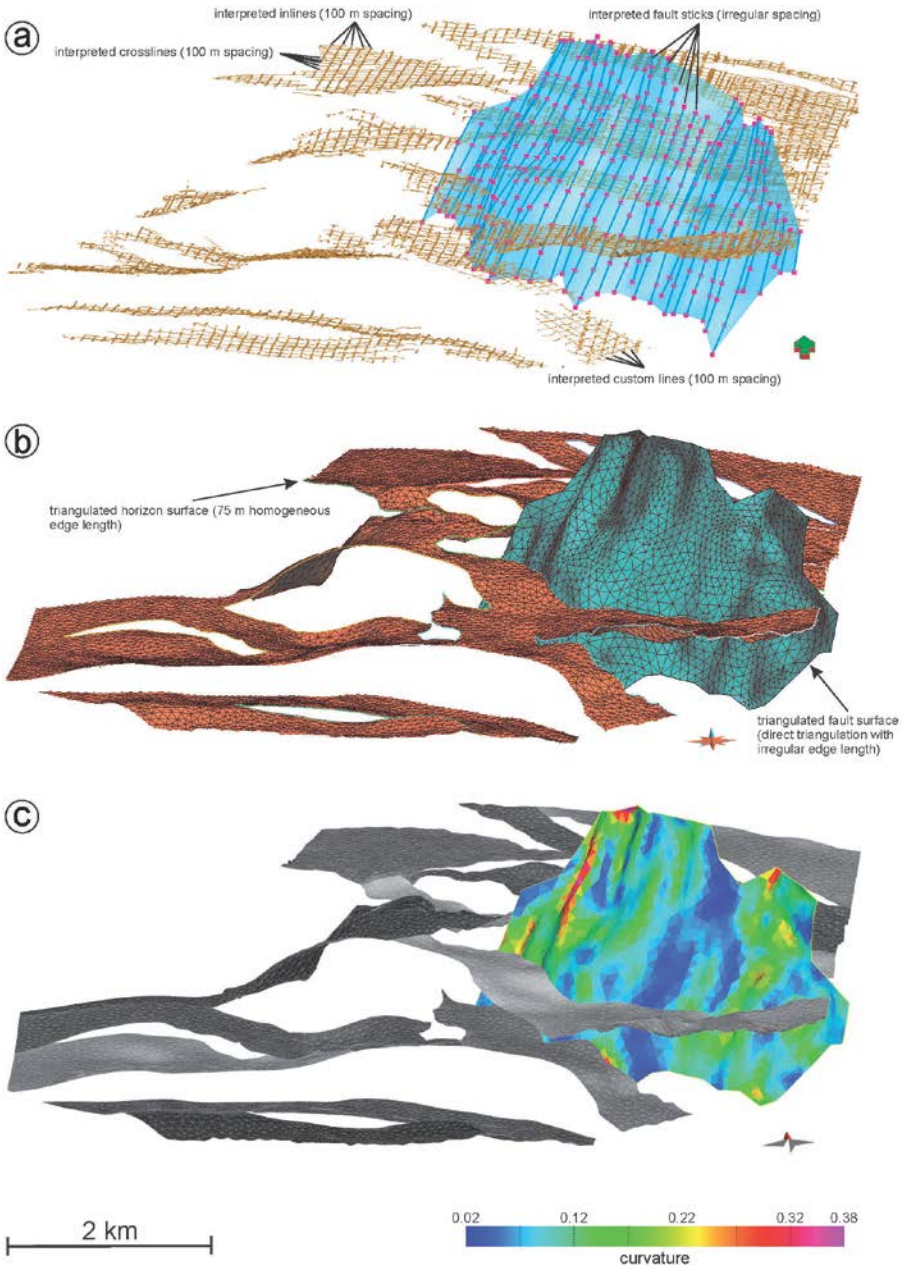

Figure 4: The three stages -seismic interpretation, model building, and structural analysis- demonstrated for one fault and the Top Waarre Fm. horizon (Fault 2; see also Figs. 6, 7, 13, 14, 15). a) Seismic interpretation showing the Top Waarre Fm. horizon picked as points on inline and crosslines, with some so-called random lines. Fault 2 was picked in detail in fault-perpendicular profiles (fault is translucent, data points in magenta). b) The same objects as irregular-triangulated surfaces. c) The same objects in the kinematic modeling software. The fault surface triangles are coloured according to curvature. See Fig. 15 for further analysis.

5 Structure of the study area

Figure 5 depicts a NE–SW seismic depth profile through the 3-D seismic cube. It shows that the subsurface of the working area can be divided into two parts: an unfaulted upper part, and a very complex and strongly-faulted lower part. The three upper stratigraphic horizons are, with their flat character, relatively similar. With increasing depth, the deformation of the horizons increases.

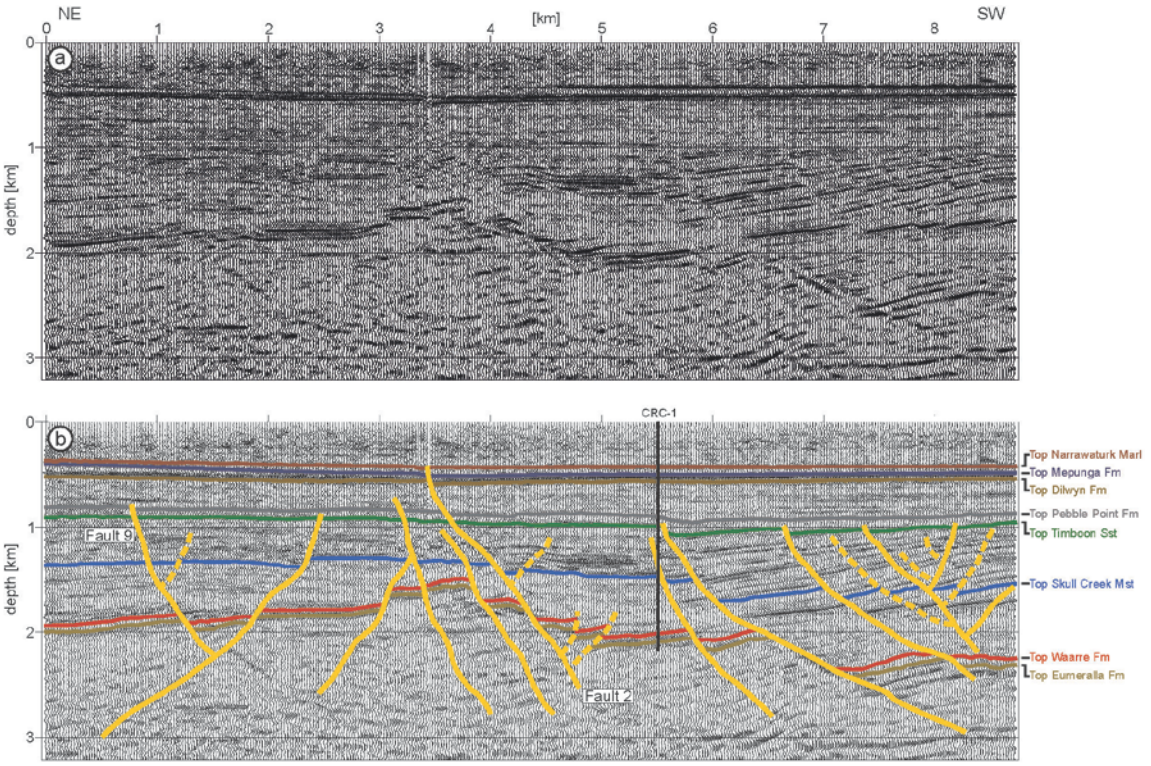

Figure 5: NE–SW seismic cross-section through the analysed area (see Fig. 1 for location). a) Depth section without interpretation. b) Interpretation of eight stratigraphic horizons, major, and minor faults (solid and dashed yellow lines, respectively). The location of CRC–1 borehole is also shown. The faults we refer to in this paper are named.

The 3-D geological model consists of eight stratigraphic horizons and 24 major faults (Fig. 6). These major faults generally dip to the SW. They are planar in the NE and become more listric towards the SW. In addition, secondary, north-dipping, antithetic faults developed due to movement on the major faults. The NW–SE-striking major faults dip by ~60° on average (Fig. 7). The dip of the listric faults in the south changes from 60–70° in the upper parts to 30–40° in the lower parts. Most faults occur below top Pebble Point Fm. at about 800 m depth. Only Fault Buttress NW and Fault 2 displace all the picked stratigraphic horizons (Fig. 6) and appear to die out in the seismically-unresolved, near-surface volume (0–450 m depth). In map-view, vertical displacements within the Waarre Fm. increase from north to south to a maximum of ~800 m (Naylor East Fault, Fig. 8a). Fault 6 and Fault Buttress South East form a horst structure (Fig. 8a & b); between these faults an enormous change (50%, 250 m) in stratigraphic thickness of the Waarre Fm. occurs (Fig. 9a). The depth-structure map of Skull Creek Fm. shows similar trends to the Waarre Fm., but the throw of the faults are significantly smaller (Fig. 8c). While the faults within the Waarre Fm. reveal throws up to 800 m (e.g., Naylor East Fault and Naylor South Fault, Fig. 8a & b), the faults within the Skull Creek Fm. reveal smaller throws up to 200 m (e.g., Naylor East Fault and Naylor South Fault, Fig. 8c & d).

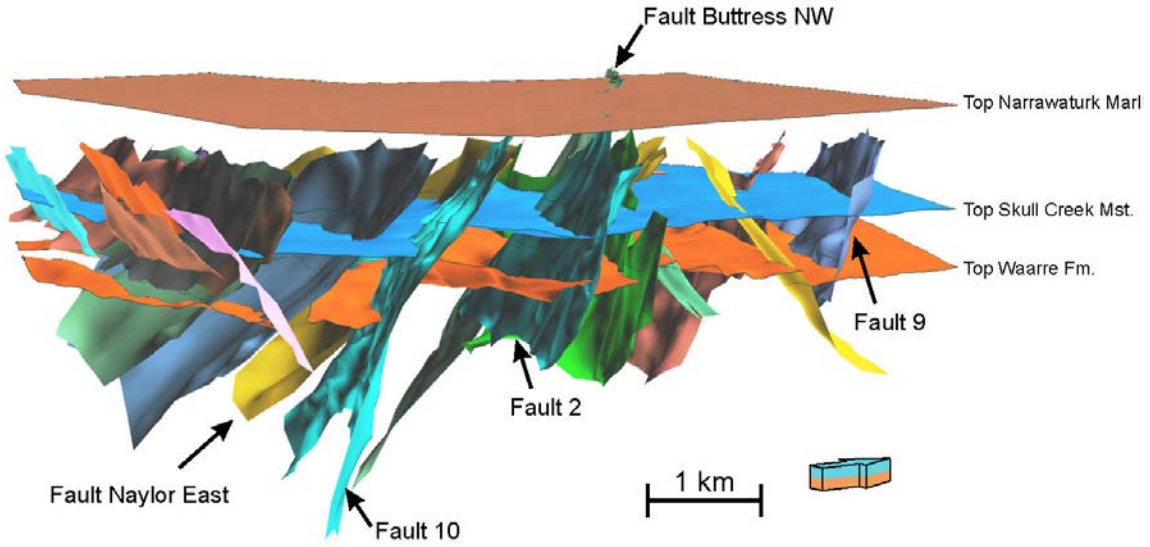

Figure 6: Oblique SE view of the complete structural model, showing 24 major faults, and, from top to bottom, the Top Narawaturk Marl, Skull Creek Mst., and Waarre Fm. horizons. The faults we refer to in this paper are named. All horizons and faults can be displayed along custom sections or layers in the supplementary 3-D PDF.

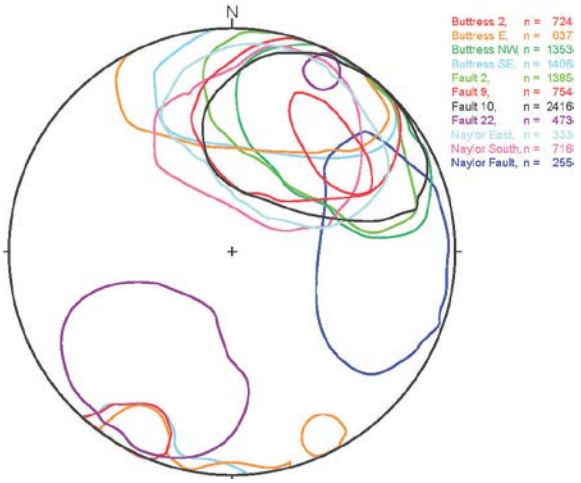

Figure 7: Isolines of the densities greater than 1% of the uniform distribution of poles to triangles that make up the fault surfaces, colour-coded by fault. Lower hemisphere projection.

A detailed study of the Top Waarre Fm. horizon show different types of fault connections (Fig. 8a, b and supplementary 3-D PDF). Hard-linked fault connections such as antithetic conjugate faults, are present only in the Skull Creek, Waarre and Eumeralla Fms. Soft-linking features, such as relay ramps, are equally distributed over the entire working area, across several stratigraphic horizons, from Top Eumeralla Fm. up to Top Pebble Point Fm.

A relay ramp connects adjacent footwalls and hanging-walls of trains of faults in a fault zone. They thus transfer the displacement between overstepping fault segments (Peacock & Sanderson, 1994). The displacement on the hanging-wall fault segment within a left-stepping relay zone increases towards the left, whereas the displacement

of the footwall fault segment decreases towards the left. The depth-structure maps of the Waarre Fm. and Skull Creek Fm. show exclusively left-stepping relay ramps (Fig. 8a & c). The overlap length of the two fault segments ranges between 20% and 40% of the total fault length. Fault segments that dip towards the south, are predominantly left stepping (Fig. 8b & d). The width of the relay ramps increases from ca. 440 m in the north up to ca. 770 m in the south. The surfaces of the relay ramps dip between 15° and 30°.

The 3-D model shows that Cretaceous sedimentary rocks have strong intraformational thickness changes (Fig. 9a, b & supplementary 3-D PDF). Isopach maps of four principal stratigraphic formations in the investigated area are depicted in Figure 9. The isopach map of the seal formation (Top Waarre Fm.–Top Skull Creek Fm.) shows strong thickness variations across the faults (Fig. 9a). For some faults, the thickness of the seal in the hanging-wall is up to four times the thickness of the footwall, which is indivative of syn-sedimentary faulting. For almost every stratigraphic horizon syn-sedimentary normal faults can be observed. The stratigraphic horizons above the seal also show strong fault growth strata and a thickness increase towards the SW (Fig. 9a & b). Within the Dilwyn Fm. the thickness trend is rotated by 90° to NW–SE (Fig. 9c). For the Dilwyn Fm. the smallest thicknesses are in the NW. The fault growth strata continue up to the Narrawaturk Marl. Due to the seismically-unresolved section above the Narrawaturk Marl, we could not continue the thickness analysis further upwards.

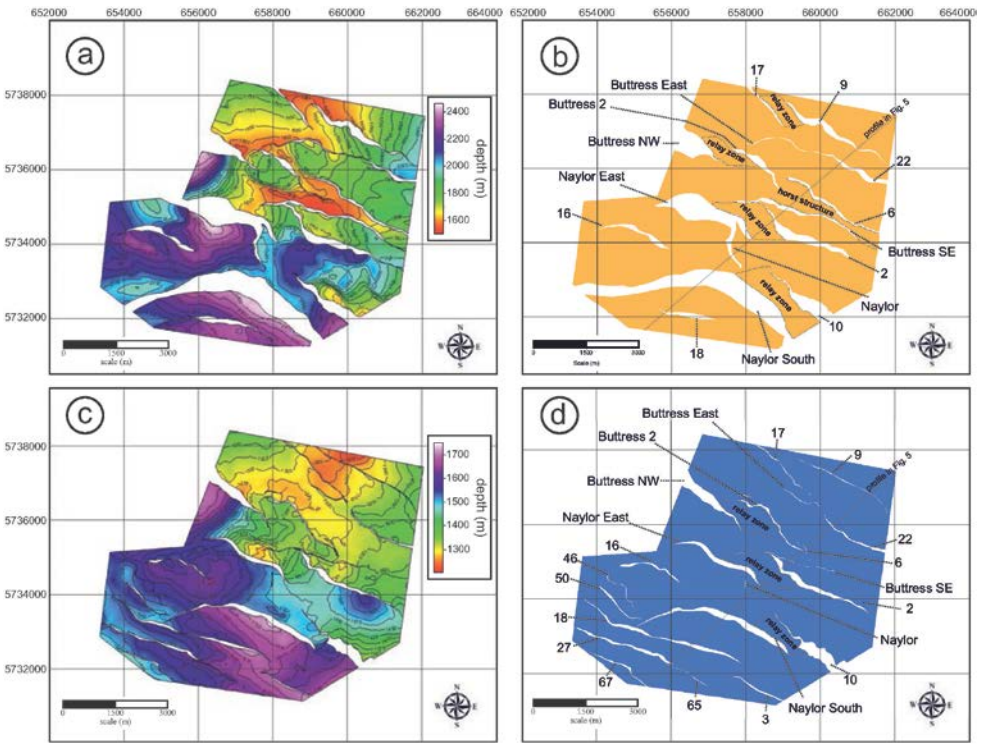

Figure 8: Depth structure and fault polygon maps for two seismic horizons: a) and b) Waarre Fm.; c) and d) Skull Creek Fm. Fault heave polygons are shown in white. Relay zones are discussed in the text.

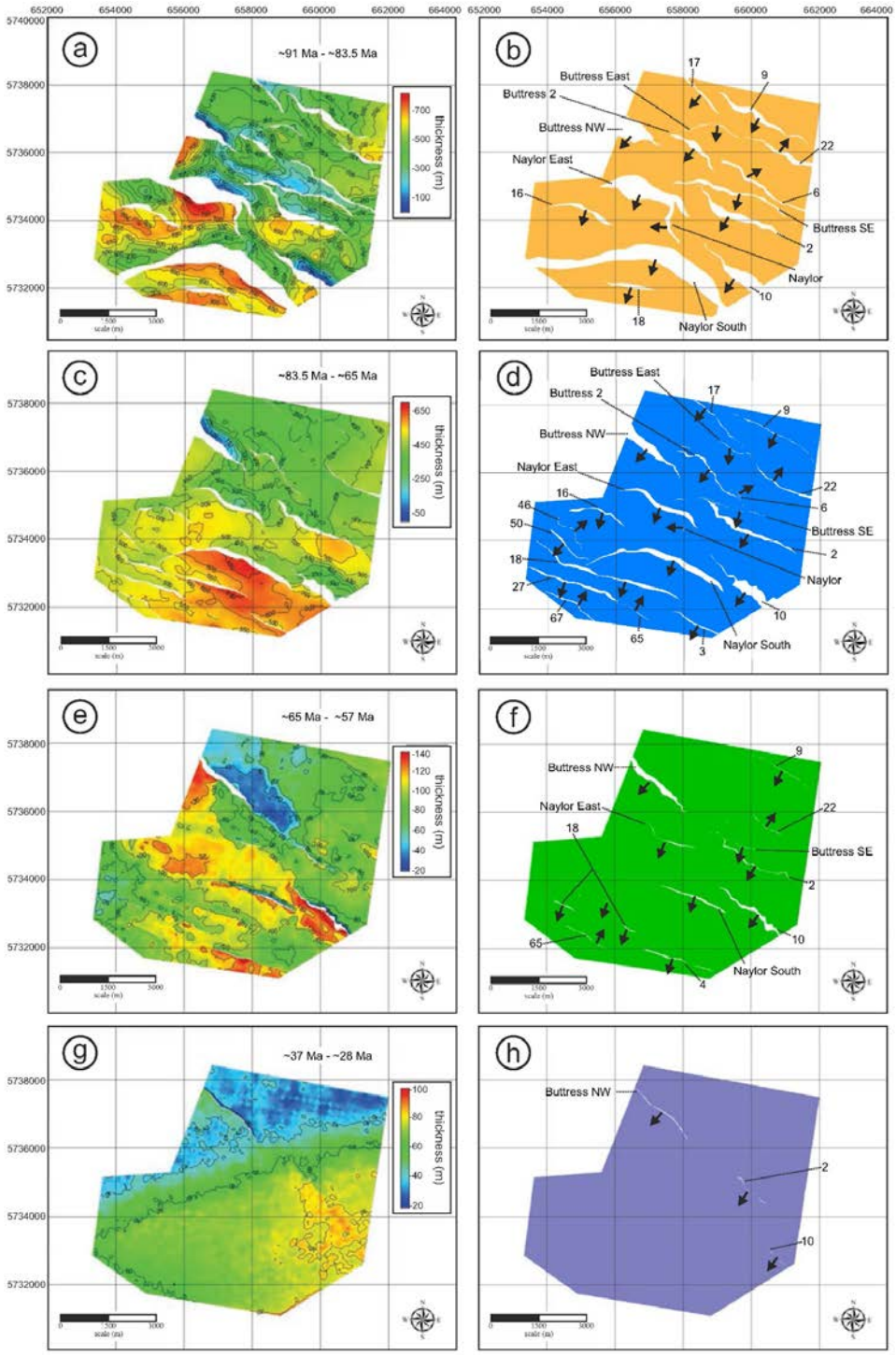

Figure 9: Isopach (a, c, e, g) and depth structure maps (b, d, f, h) of different stratigraphic formations to illustrate sediment thickness change, fault activity, and fault growth strata. Arrows on depth maps show fault dip direction. a) and b) Top Waarre Fm. to Top Skull Creek Mst: highly faulted, strong fault growth strata, sedimentary thicknesses increase towards the southwest. c) and d) Top Skull Creek Fm. to Top Timboon Fm: highly faulted, strong fault growth strata, sedimentary thicknesses increase towards the southwest. e) and f) Top Timboon Fm. to Top Pebble Point Fm: less faulted, significant fault growth strata at faults Buttress NW, 10, Naylor South, and 4; higher sedimentary thicknesses to the southwest. g) and h) Top Mepunga Fm. to Top Narrawaturk Fm: two faults were active, weak fault growth strata, sedimentary thicknesses increase in this case towards the southeast.

6 Kinematic analysis of selected faults

6.1 Style and timing of fault growth

To specify the temporal development of the normal faults, the Allan maps (Fig. 10a, Fig. 11a) and throw-depth diagrams (Fig. 10b, Fig. 11b) of different stratigraphic horizons are plotted within one figure. Figure 10a shows the Allan maps of Fault Naylor South combined with Fault 10, because the two faults are connected via a relay zone. In both Allan map diagrams the amount of displacement decreases upwards, i.e. towards younger strata. Throw-depth plots were created to analyse the decrease in throw in detail and to characterise the fault activity (Tvedt et al., 2013). The maximum throw of Fault 10 is 800 m at the Top Eumeralla and Top Waarre Fms., 260 m at the Skull Creek Mst., and 50 m at the Pebble Point Fm. (Fig. 10b, Profile 5). Fault Naylor South show smaller throws than Fault 10, but the same trend. On both faults the displacement is typically greatest at the Top Waarre or Top Eumeralla Fms. (Fig. 10b). This significant change in throw over time shows that displacement on the Fault Naylor South and Fault 10 continually waned until deposition of Pebble Point Fm. The Fault Naylor South and Fault 10 are soft-linked by a SE-dipping relay zone that is unbreached at all structural levels. The Allan maps of both faults cross-cut between 3500 and 4400 m fault strike length. The thick black lines represent the fault tip lines of both faults and thus indicate the dimension of the relay zone. The relay zone occurs at all interpreted stratigraphic levels and has a maximum length of 500 m. Its width gradually decreases upwards.

A detailed study of the Allan maps and throw-depth plots of Fault Naylor East and Fault 2 (Fig. 11a) shows similarities as well as differences to Fault Naylor South and Fault 10. The Fault Naylor East behaves similarly to Fault 10, with a maximum throw up to 900 m of the Top Eumeralla Fm. The amount of displacement decreases continually upwards.

Note also the large displacement only within the hanging-wall of Waarre and Eumeralla Fms. of Fault Naylor East at 2000 to 2150 m fault strike length. This is caused by the abutting Naylor Fault (Fig. 8).

The displacement of all stratigraphic levels of Fault 2 is considerably smaller than Fault 10. The very small displacements relates to Fault Buttress SE that is directly in the footwall of Fault 2 and takes on the bulk of the displacement (dashed lines in Fig. 11b, see 3-D PDF). These two faults are also soft-linked by a relay zone. This relay has a width of about 700 m and maintains this width, in contrast to the relay zone of Figure 10, up to Top Timboon Sst. Only within the Pebble Point Fm. does the relay zone become significantly smaller.

These two examples show that the faults have asymmetric throw profiles at all stratigraphic levels, where the throw within the relay ramp decreases more abruptly than compared to the opposing fault tip. This would suggest kinematic interaction between the faults in the relay zone (e.g., Imber et al., 2004; Long & Imber, 2012; Walsh et al., 1999). This could be due to deformation being taken up by the rotation of the relay ramp or unresolved small scale damage within the relay zone (e.g., Peacock & Sanderson, 1994).

6.2 Fault morphology

We analysed the morphology of the fault surfaces from the detailed 3-D seismic interpretation to obtain possible information about fault kinematics. The 3-D model (Fig. 6; supplementary 3-D PDF) shows that the faults possess distinct morphology. By using different attributes (curvature, cylindricity) we are able to highlight the corrugations on the fault surfaces. These corrugations are real, rather than interpretation artifacts (e.g., Needham et al., 1996b; Lohr et al., 2008). We observed morphology on most of the faults (supplementary 3-D PDF). Needham et al. (1996b) suggested that abrupt topographic variations on the fault surface should be checked. Therefore we used random lines (sec. 4.1) on all faults to verify the fault morphology and exclude

misinterpretations. Alternatively, they can be investigated using variance maps. Figure 12 shows the variance maps for three faults of different time-slices. These three faults exemplify the fact that our interpreted major faults have real corrugations. The variance maps of Fault 9 (Fig. 12a–c) show that two fault segments form a very small relay zone (Fig. 12a, at the kinks). Fault Naylor South has the form of a sickle and shows few corrugations that are detectable in high resolution of the variance. The small gap of the upper end of Naylor South Fault (Fig. 12d) fits with the fault interpretation, because in this part the fault interpretation didn't reach that depth, i.e. it tips out beneath this level.

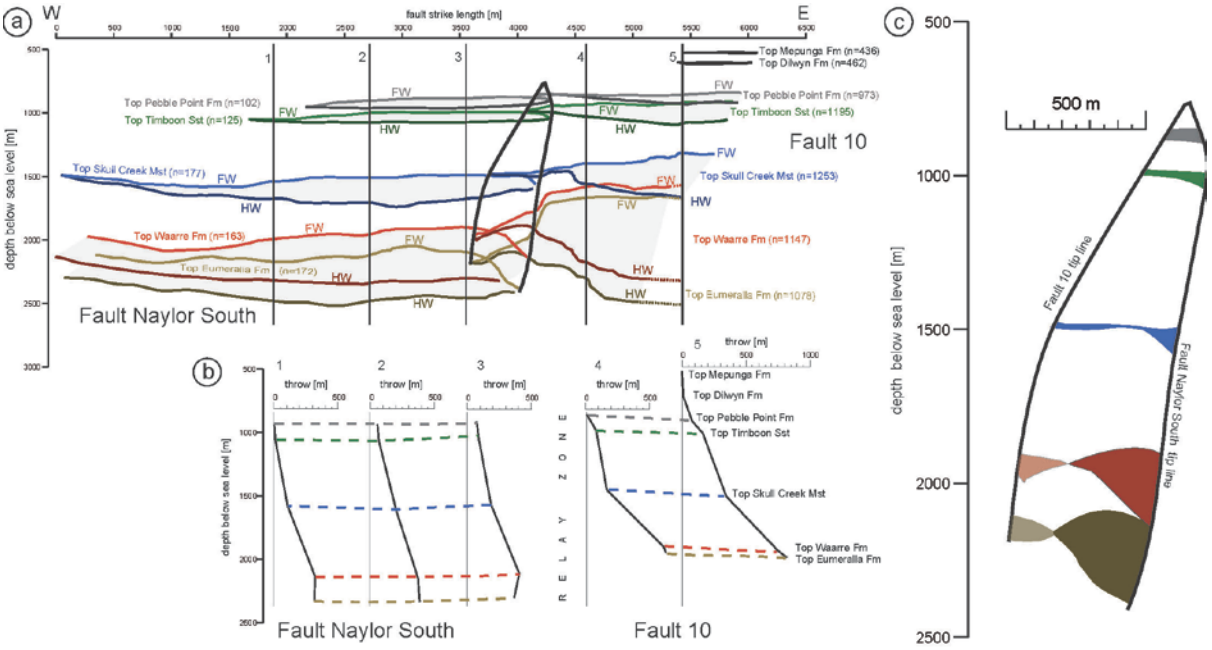

Figure 10: Allan maps and throw-depth plots of Naylor South Fault and Fault 10 showing the throw of the juxtaposed strata. Stratigraphic horizons are colour-coded. a) Allan maps. The amount of juxtaposition decreases stratigraphically upwards. Footwall (FW) and hanging-wall (HW) are depicted with different colour intensities, black lines represent the fault tip lines and thus the dimension of the relay zone in between. b) Throw-depth plots of Fault Naylor South and Fault 10 in the calculated kinematic direction (see section 6.2). Location of sections are shown in a). c) Enlargement of the relay-zone, showing its structure.

The corrugations of Naylor East Fault have the form of cuspate-lobe structures (Fig. 12g–h) that resulted from fault segmentation. A comparison of averaged fault surfaces (with 300 m edge length) with the original triangulated fault surfaces (with 75 m edge length) provides information about the geometries of the corrugations. Histograms of three faults show the magnitude-difference between the original fault surface and the averaged fault (Fig. 13a–c). All histograms have more or less an exponential character (Fig. 13a–c). This means that the change in angle of the curvature of the corrugations is smooth. Although the triangle edge length of the averaged fault surfaces has more than doubled, the counts above the seismic resolution of 25 m show the existence of corrugations in this scale.

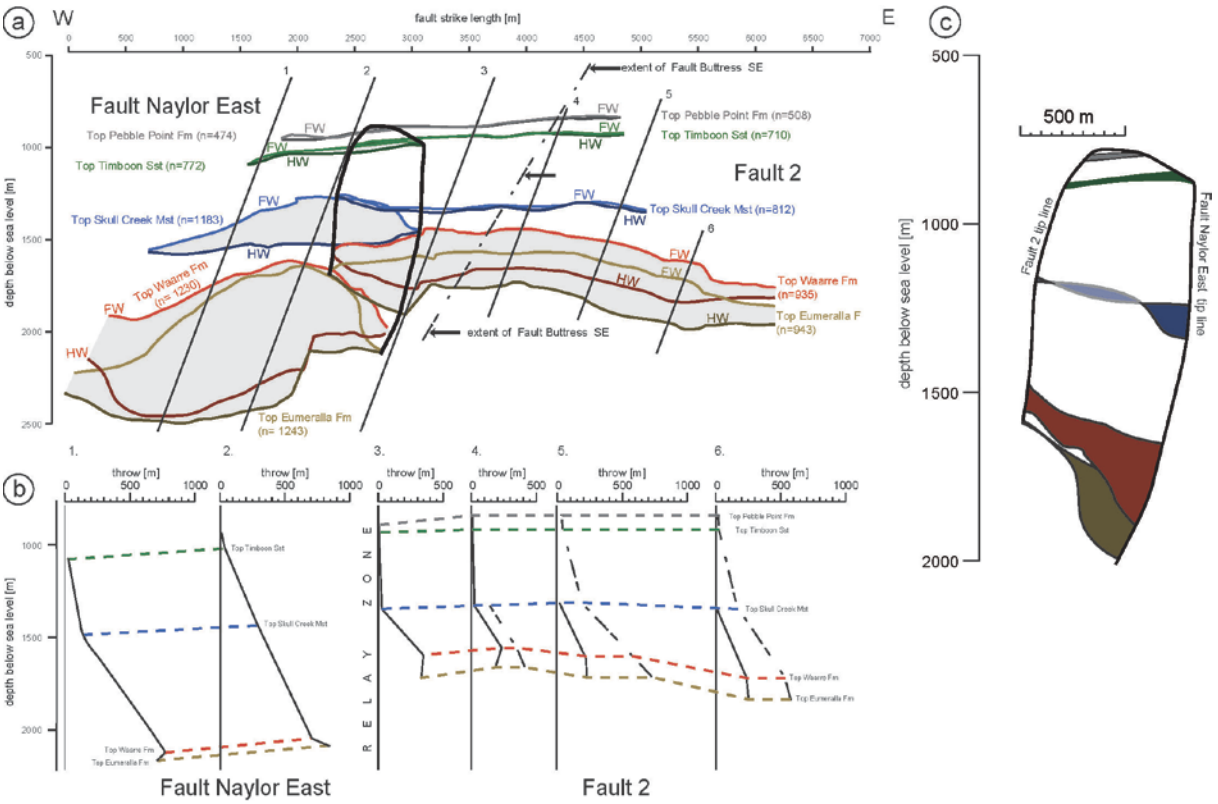

Figure 11: Allan maps and throw-depth plots of Fault Naylor East and Fault 2 showing the throw of the juxtaposed strata. Stratigraphic horizons are colour-coded. a) Allan maps. The amount of juxtaposition decreases upwards, i.e. towards younger strata. Note that the displacement of all stratigraphic levels of Fault 2 is considerably smaller. This relates to Fault Buttress SE that is directly in the back of Fault 2 and takes the large displacements over (dashed line). Footwall (FW) and hanging-wall (HW) are depicted with different colour intensities, black lines represent the fault tip lines and thus the dimension of the relay zone in between. b) Throw-depth plots of Fault Naylor East and Fault 2 in the calculated kinematic direction (see section 6.2). Location of sections are shown in a). c) Enlargement of the relay-zone, showing its structure.

The corrugation dimensions were quantified by measuring the length-width ratios of corrugations of four major faults (Fig. 14). The corrugation lengths range between 500 and 2800 m and the width (half wavelength) varies between 100 and 500 m. For all faults, the corrugations are approximately elongated in the fault dip-direction (supplementary 3-D PDF).

To quantify the corrugations further, curvature and cylindricity attributes of the fault surfaces were calculated. While curvature recognises the magnitude of the corrugation, cylindricity defines its orientation (Lohr et al., 2008). Figure 15 shows four examples of curvature and cylindricity attributes plotted on the surfaces of the faults: 2, 10, Buttress SE, and Buttress 2. Curvature of all faults (top of Fig. 15a) shows flat parts (lower values of 0.01–0.09) and corrugations (higher values of 0.21–0.46). For example, the mean cylindrical axis of Fault 2 dips 57°/N235°E, whereas the lower hemisphere projection of poles to triangles (Fig. 15c) shows the fault plane has a mean dip direction of 61°/N211°E. Consequently, the cylindrical long axis of Fault 2 is rotated clockwise by 24° with respect to the fault plane azimuth (i.e. N211°E from N235°E). This corresponds to a change in rake of 8° towards the west. The results of orientation and cylindricity analyses on all major faults in the study area are depicted in Figure 16. About 60% of the faults show that the direction of cylindricity is parallel to the dip direction of the fault planes. However, the remaining faults' cylindrical axes are rotated clockwise by up to 24° as shown for Fault 2.

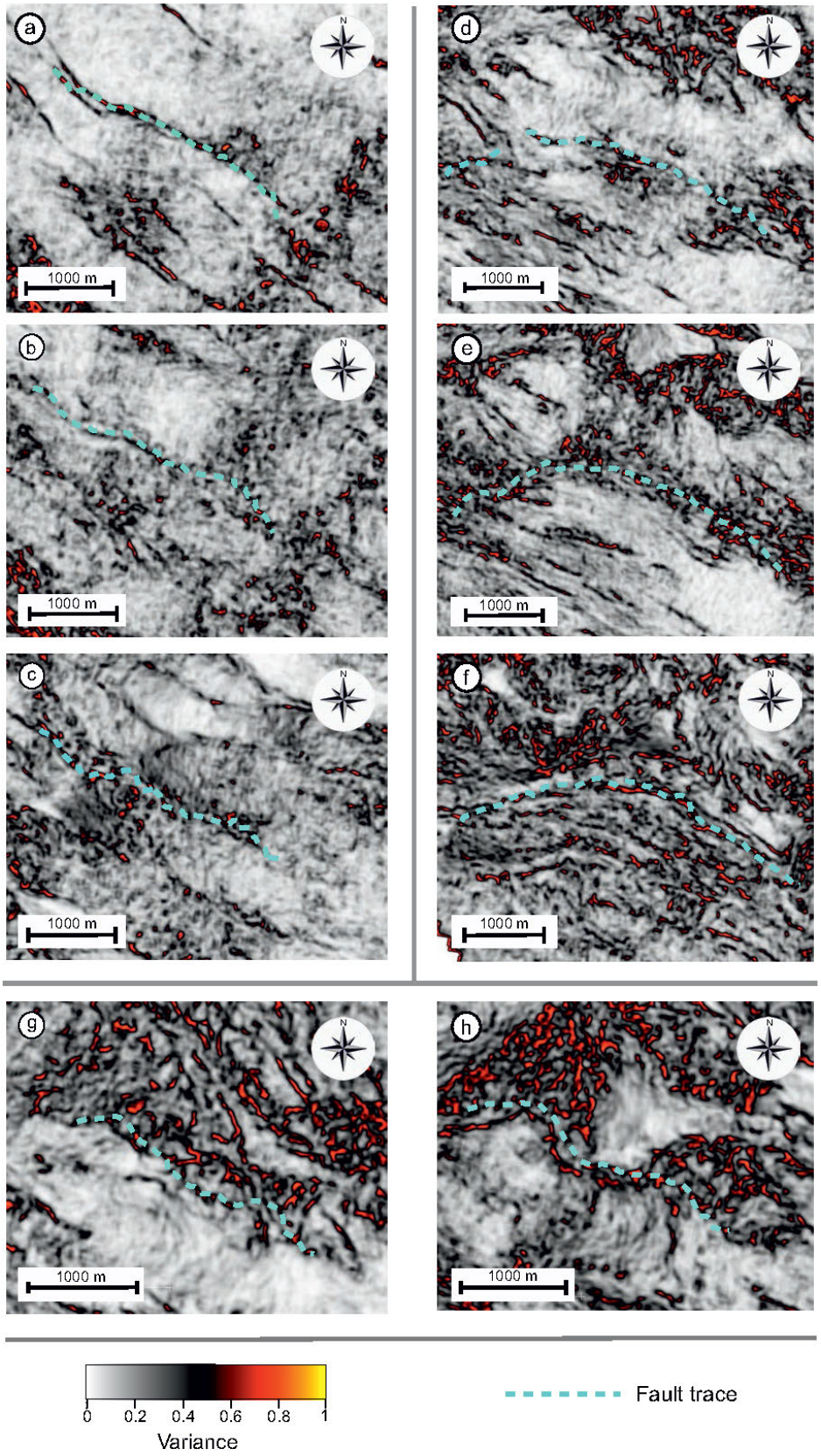

Figure 12: Variance maps with fault traces at different time slices. a) Fault 9 time: -969 ms /depth: -1101 m; b) Fault 9 time: -1160 ms /depth: -1405 m; c) Fault 9 time: -1308 ms /depth: -1653 m; d) Naylor South Fault time: -1136 ms /depth: -1374 m; e) Naylor South Fault time: -1272 ms /depth: -1589 m; f) Naylor South Fault time: -1628 ms /depth: -2178 m; g) Naylor East Fault time: -1120 ms /depth: -1346 m; h) Naylor East Fault time: -1300 ms /depth: -1567 m.

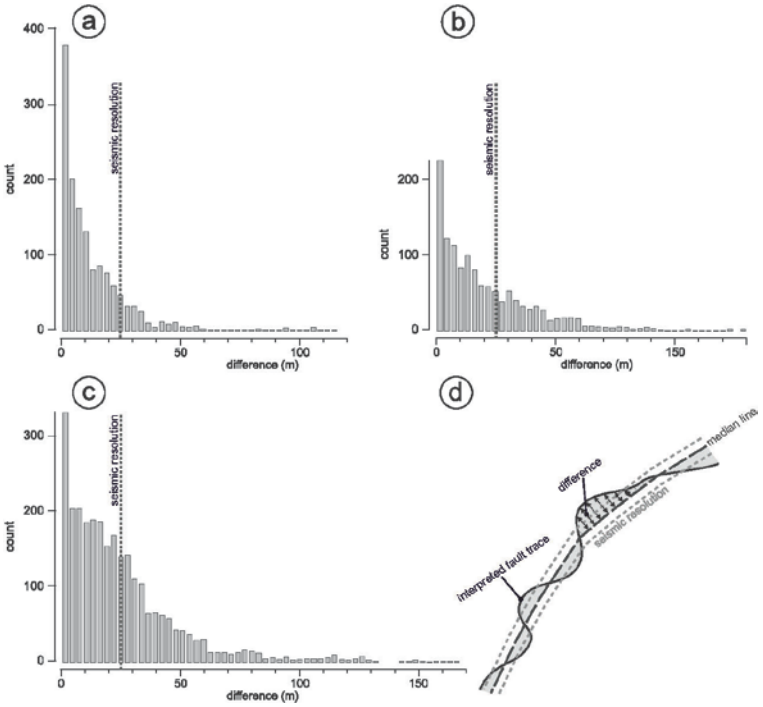

Figure 13: Comparison of the modelled triangulated fault surfaces (75 m edge length) against averaged triangulated surfaces constructed from the fault point sets with 300 m edge length. The latter surfaces therefore form a median surface through the former (d). The histograms show the difference between the modelled and averaged surfaces versus count for: a) Fault Buttress SE; b) Fault 2; c) Fault 10.

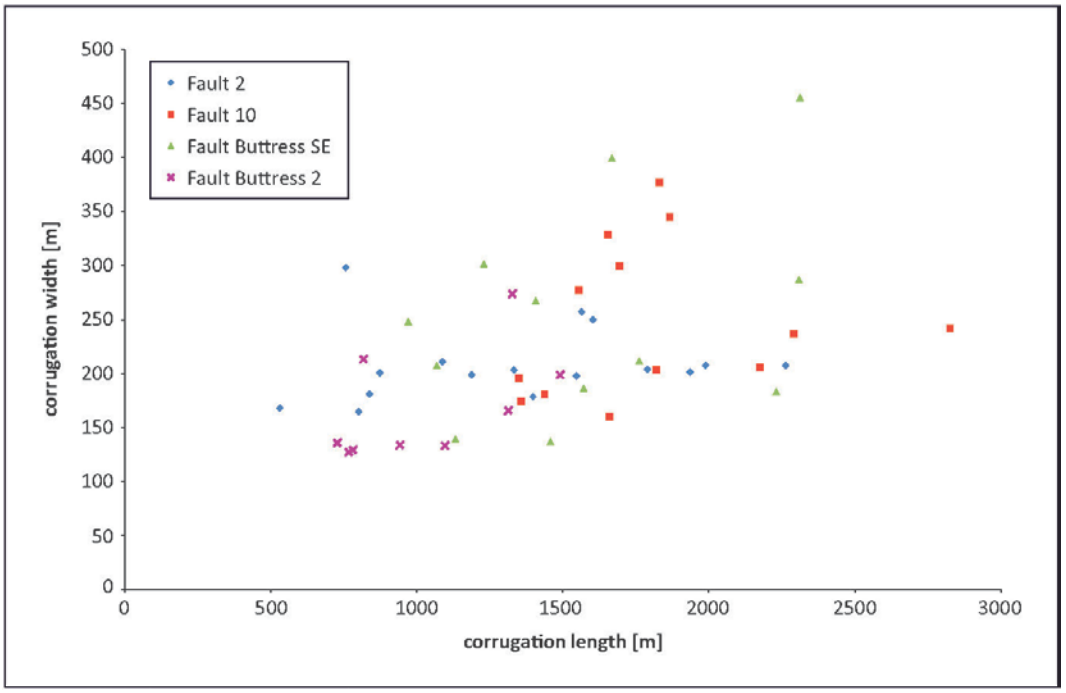

Figure 14: Length versus width plot for corrugations of four fault examples measured directly in the 3-D model. The faults' maximum length is: Fault 2 – 2598 m, Fault 10 – 4748 m, Fault Buttress SE – 2645 m and Fault Buttress 2 – 2190 m.

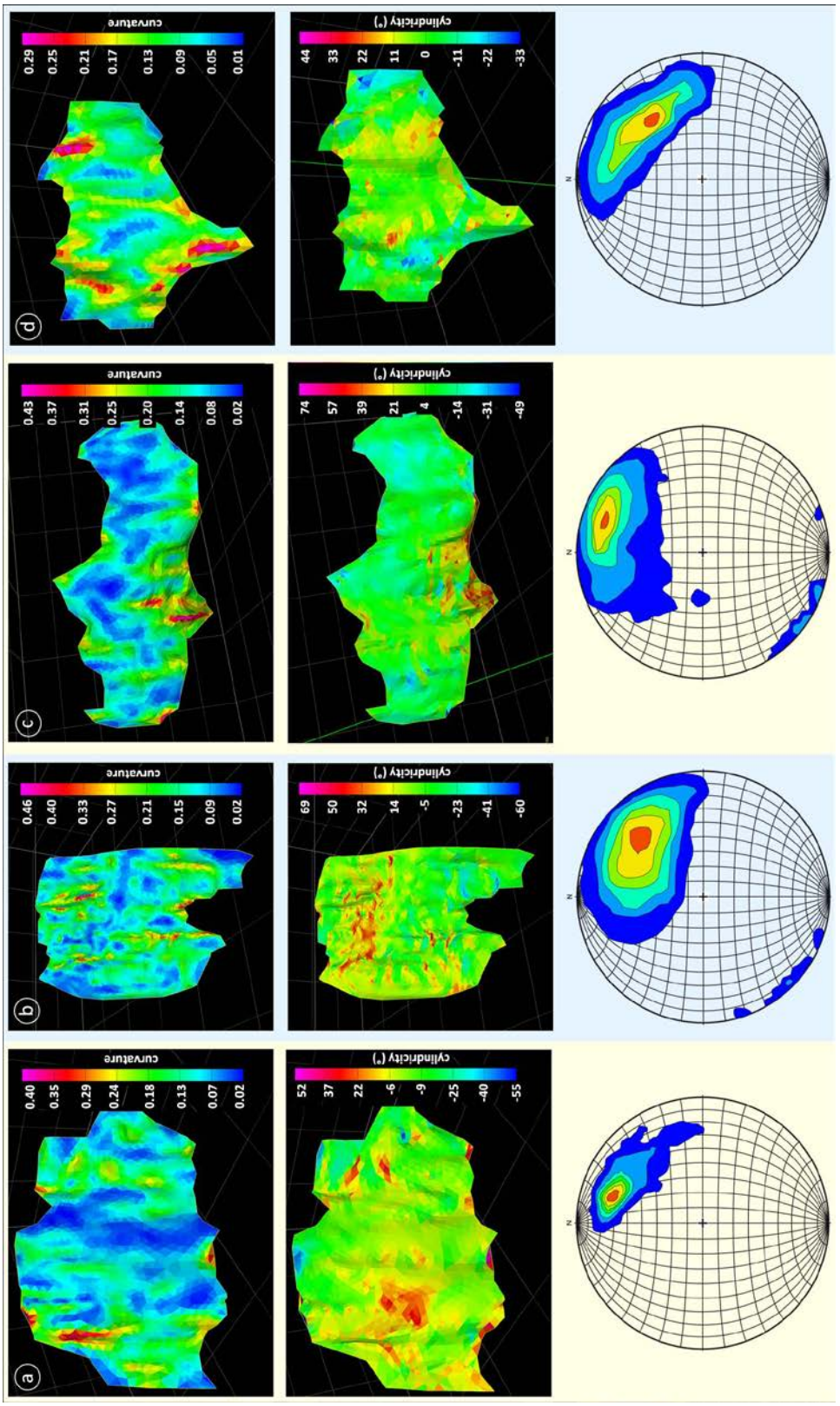

Figure 15: Structural analysis of a) Fault 2, b) Fault 10, c) Fault Buttress SE and d) Fault Buttress 2. Top: Fault surfaces are colour-coded for curvature. Note the strong, parallel linear zones of high and low curvature. Middle: Fault surfaces are colour-coded for cylindricity. Bottom: Equal-area, lower hemisphere projection of poles to triangles that make up the fault surface. Contours in integers of multiples of uniform distribution, blue — lowest, red — highest.

7 Discussion

7.1 Timing of faulting

The study area is part of the western Otway Basin (Finlayson et al., 1996; Cooper & Hill, 1997; Miller et al., 2002) and it is dominated by a complex system of E–W and NW–SE striking normal faults and subordinate NE-dipping antithetic faults. Because all major extensional faults have approximately the same strike and show similar syn-sedimentary thickness variations in the Early to Late Cretaceous strata, they presumably originated in the same tectonic phase (before 100 Ma). Secondary antithetic faults with the same strike were created in response to movement on the major faults at later stages. Major sediment accumulation against faults is typical for the southern passive margin of Australia (Fig. 2). Sediment loading led to additional subsidence and sediment accumulation as the margin moved away from the oceanic spreading centre. All sediments below Top Pebble Point Fm. (Early Eocene) were deposited syn-rift. The sediments above Pebble Point Fm. probably are post-rift, because these sediments blanket most faults, which were inactive after the Early Eocene. Only two faults in the north (Fault 2 and Fault Buttress NW) were active until the Oligocene or even later. Our observations thus fit the existing studies of the local geology (Krassay et al., 2004). Allan map analysis shows that the major faults were continually active (Fig. 10, Fig. 11), at least from Top Eumeralla Fm. (Early Cretaceous) to Top Skull Creek Mst. (Late Cretaceous), and some even higher (Eocene). We also observe that the throw significantly decreases with decreasing age. This also means that the amount of tectonic lateral extension strongly decreases upwards. Together with isopach maps this clearly illustrates syn-sedimentary behaviour and indicates strong fault control on deposition.

7.2 How can corrugations provide information about fault kinematics?

Nearly all interpreted faults in our study area show corrugations that occur over the entire surface of the fault. We exclude that these structures are interpretation artifacts, because we observe curved segments of the faults at different stratigraphic levels that can be correlated between horizons (Fig. 12). Normal faults, such as those in this area, presumably developed from individual fault segments that grew upwards and laterally coalesced (Childs et al., 1996; Mansfield & Cartwright, 2001; Walsh et al., 2003). We postulate that when two curved segments coalesce, the suture between them cannot be easily destroyed; instead the suture propagates upwards in the movement direction as the fault grows. Figure 12 shows that faults consist of a number of curved segments at different depth levels. The fault surfaces are therefore characterised by corrugations, which are parallel to sutures between the fault segments and, we postulate, the kinematic vector, i.e. movement direction on the fault. Needham et al. (1996b) also observed real corrugation of normal fault surfaces and related this to the slip vector on the fault surface. Resor & Meer (2009) used a LiDAR scan of a 70 m high outcrop of the Arkitsa normal fault surface in Greece to demonstrate that it exhibits corrugations on 2–50 m wavelengths that significantly stretch over the entire fault surface in the slip direction. Awdal et al. (2014) recognised deformation-band lozenges in sandstone-outcrops from the Moray Firth (Scotland) and southeastern Utah (USA). They analysed deformation-band lozenges over different scales (length between 10 and 100000 mm), thus above seismic resolution. While the lozenges have an oblate or rhomboidal-shape, the corrugations of the faults in the study area have a more elongated shape.

We draw information about the fault kinematics from two different analyses:

1. Relay ramps are equally distributed over the entire area, within Top Eumeralla Fm., Top Waarre Fm. and Top Skull Creek Fm. We observed that all relay ramps are left-stepping. However, the size of our

study area allows only the relationship between two or three faults along strike to be analysed in this fashion. Nevertheless, we suggest that this may indicate a dextral sense of shear (Fig. 8).

2. By using dip, azimuth, curvature and cylindricity attributes of the morphology of the fault planes we are able to quantify the direction of movement along the fault surface, parallel to the long axis of cylindricity. Curvature reflects the amplitude of fault corrugation while cylindricity estimates orientation (Fig. 15).

For approximately 60% of the faults the trend of corrugations is parallel to the azimuth of the fault surface. This infers that displacement was primarily dip-slip (Fig. 16). However, for the other 40% of the faults we identified clockwise rotation of the faults' cylindrical axes by up to 25°, which we infer as a local dextral oblique slip component. Nevertheless, there is no particular area with asymmetrical faults, rather they are distributed equally between the dip-slip faults (Fig. 16). This suggests strain partitioning on the scale of the working area, at least during the major phase of extension in the Cretaceous.

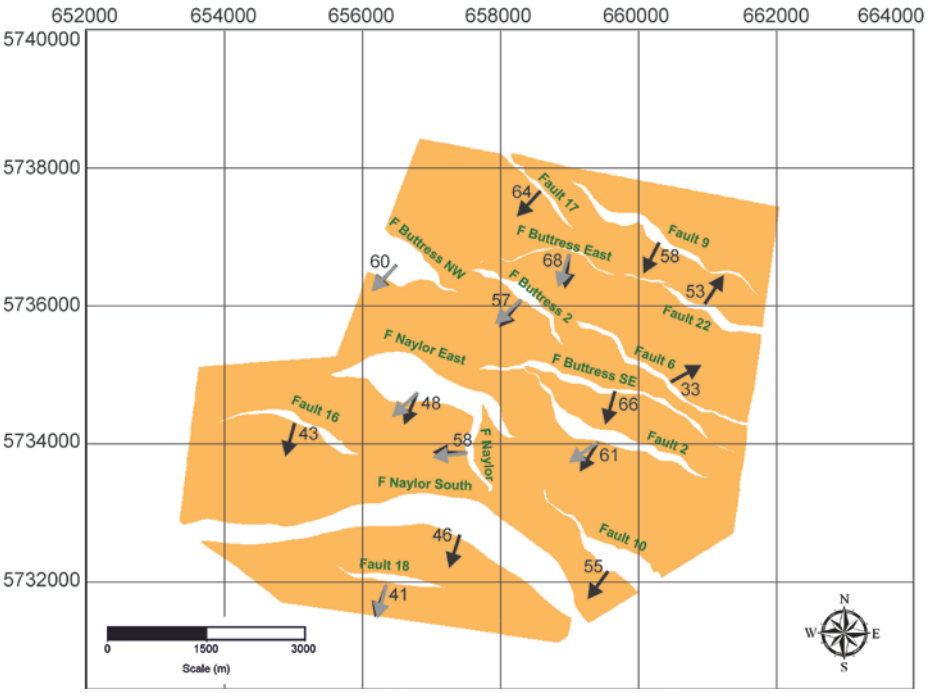

Figure 16: Map of the Top Waarre Fm. horizon. Black arrows and values represent the average dip direction and dip of the faults. Grey arrows indicate the directions of cylindricity vectors from the structural analysis (see Fig. 15 and text for details). Note that grey arrows are either equal to the dip direction or rotated clockwise by up to 25°.

7.3 Implications of this work for the Otway Basin

This work contributes to detailed fault analysis as well as fault kinematics of the Otway Basin. The detailed knowledge of the transport direction during faulting helps to reconstruct the paleogeography correctly and with the construction of balanced cross-sections. In order for a 2-D balanced cross-section to restore properly it must be constructed in the transport direction or at least the deviation of the transport vector and the profile direction must be known (Woodward et al., 1986; von Winterfeld & Oncken, 1995). Our results support Perincek & Cockshell (1995) who suspected dextral oblique slip movement in the western Otway Basin, but were not able to

show evidence of such. Our methods allow us quantify the amount of the dextral oblique slip component on each individual fault. Most faults show dip-slip movement, but 40% of the analysed faults have a dextral oblique slip component. Krassay et al. (2004) described the tectonostratigraphic evolution of the Otway Basin using paleostratigraphic methods and determined a change from extension during late Cretaceous to a combination of subsidence with a local phase of inversion until the end of the Palaeogene. On the basis of the structural analysis shown in this paper, we postulate that strong subsidence was continuous during the Cretaceous. Subsequently the amount of subsidence and extension steadily decreased until Top Narrawaturk Marl (~ 28 Ma). Both the Allan maps and throw-depth plots show that the majority of the faults died out in the Pebble Point Fm. (~ 57 Ma), which coincided with the opening of the Southern Ocean (Norvick & Smith, 2001). Presumably, the formation of true oceanic crust released the stresses in the Otway Basin that had been responsible for the faulting until this time (Palaeogene). Eight hundred metres of sedimentary rocks were deposited after 57 Ma with only three active faults. This suggests subsidence from this point onwards was dominated by thermal relaxation.

8 Conclusions

We developed a detailed geological 3-D model of an 8 km×7 km area around the CO2CRC Otway project site built from a detailed 3-D seismic interpretation. The model consists of eight stratigraphic horizons and 24 major faults. The area is part of the western onshore Otway Basin, which is a rifted passive margin. The 3-D model reflects the typical thick sediment accumulation and listric normal faulting that occurs in such a tectonic setting. We carried out structural analysis of the faults and conclude:

1. Fault connections: The identified fault system has two types of fault connections: 1) hard-linked features, such as subordinate antithetic faults. 2) relay ramps acting as soft-linking fault connections, which occur only within Cretaceous sediments, but are distributed over the entire area. The widths of the relay ramps increase towards the south, i.e. towards the spreading margin.
2. Fault activity: Based on Allan map and isopach map analysis we show fault growth strata and how fault throw decrease over time. Most major faults were constantly active from Early Cretaceous until Late Paleocene (~ 57 Ma). Two faults in the northern part of the study area were active until the Oligocene or even later. Because we cannot resolve structures above Narrawaturk Marl Fm. in the 3-D seismic, it is possible that the faults reach even higher, possibly up to surface. To prove this, an additional near-surface seismic study is required.
3. Fault kinematics: Left-stepping relay ramps, and fault attributes such as cylindricity and curvature show a component of dextral oblique slip movement for 40% of the faults. In the latter cylindrical axes are rotated up to 25 degrees clockwise with respect to the fault azimuth. The rest of the faults show dip-slip movement. The faults with a oblique slip component are equally distributed over the study area. This would suggest strain partitioning took place, although the study area is only a small part of the Australian Otway Basin.

In summary, our study uses structural analysis on a 3-D model built from detailed 3-D seismic interpretation to give detailed insight into fault behaviour and regional tectonics. With powerful tools such as Allan map analysis, isopach maps, curvature and cylindricity, the fault history, activity, connectivity, and kinematics can be quantified. Especially the investigation of fault corrugations can help to distinguish the kinematic vector of fault movement that is important for both applied exploration and basic basin studies.

Acknowledgements

We thank Neeske Luebben and Nicole Duda for their assistance in creating some of the figures. We are especially grateful to Mark-Fabian Slaby, Rüdiger Reimann, and colleagues from the German State Authority for Mining, Energy and Geology in Lower Saxony for creating the 3-D PDF. Christopher Jackson, Casey Nixon, and Andrew Nicol are thanked for their very constructive reviews of the manuscript. We thank Midland Valley for an academic license for Move. This work was sponsored in part by the Australian Commonwealth Government through the Cooperative Research Centre for Greenhouse Gas Technologies (CO2CRC). PROTECT is funded through the Geotechnologien research programme in Germany (grant 03G0797, publication number: GEOTECH-2215).

Conflict of interest

No conflict of interest declared.

References

ALLAN, U.S. (1989) Model for hydrocarbon migration and entrapment within faulted structures. AAPG Bull, 73, 803–811.

ALLEY, N.F. & LINDSAY, J.M. (1995) Tertiary. In: DREXEL, J.F. & PREISS, W.V. (Eds.), The geology of South Australia, Vol. 2. Geological Survey of South Australia.

ARUFFO, C.M., RODRIGUEZ-HERRERA, A., TENTHOREY, E., KRZIKALLA, F., MINTON, J. & HENK, A. (2014) Geomechanical modelling to assess fault integrity at the CO2CRC Otway Project, Australia. Australian J. of Earth Sci., 61, 987–1000.

AWDAL, A., HEALY, D. & ALSOP, I.G. (2014) Geometrical analysis of deformation band lozenges and their scaling relationships to fault lenses. Journal of Structural Geology, 66, 11–23.

BÉRARD, T., SINHA, B.K., VAN RUTH, P., DANCE, T., JOHN, Z. & TAN, C. (2008) Stress estimation at the Otway CO2 Storage Site, Australia. SPE Asia Pacific Oil and Gas Conference and Exhibition, 26, 135–148.

BLEVIN, J.E. & CATHRO, D.L. (2008) Australian Southern Margin Thesis - Project GA707, Client report to Geoscience Australia by FrOG Tech Pty Ltd. GeoCat 68892. Technical report.

BRANDES, C. & TANNER, D.C. (2012) Three-dimensional geometry and fabric of shear deformation-bands in unconsolidated Pleistocene sediments. Tectonophysics, 518-521, 84-92.

BRYAN, S.E., CONSTANTINE, A.E., STEPHENS, C.J., EWART, A., SCHOEN, R.W.
& PARIANOS, J. (1997) Early Cretaceous volcano-sedimentary successions along the eastern Australian continental margin: Implications for the break-up of eastern Gondwana. Earth and Planetary Science Letters, 153, 85–102.

CARTWRIGHT, J.A., TRUDGILL, B.D. & MANSFIELD, C.S. (1995) Fault growth by segment linkage: an explanation for scatter in maximum displacement and trace length data from the Canyonlands Grabens of SE Utah. Journal of Structural Geology, 17, 9, 1319-1326.

CGG AUSTRALIA PTY. LTD. (2000) Final Report Seismic Data Processing OCV00 Curdie Vale 3D. Technical report, CGG Australia Pty. Ltd., PO Box 371, West Perth, WA 6872.

CHILDS, C., NICOL, A., WALSH, J.J. & WATTERSON, J. (1996) Growth of vertically segmented normal faults. Journal of Structural Geology, 18, 12, 1389–1397.

CONTRERAS, J., ANDERS, M.H. & SCHOLZ, C.H. (2000) Growth of a normal fault system: observations from the Lake Malawi basin of the east African rift. J. Struct. Geol., 22, 159–168.

COOK, P.J. (Ed.) (2014) Geologically Storing Carbon: Learning from the Otway Project Experience. CSIRO Publishing, Melbourne, 384p.

COOPER, G.T. & HILL, K.C. (1997) Cross-section balancing and thermochronological analysis of the Mesozoic development of the eastern Otway Basin. The APPEA Journal, 153, 390–414.

DANCE, T. (2013) Assessment and geological characterisation of the CO2CRC Otway Project CO2 storage demonstration site: From prefeasibility to injection. Marine and Petroleum Geology, 46, 0, 251–269.

DAWERS, N.H. & UNDERHILL, J.R. (2000) The role of fault interaction and linkage in controlling syn-rift stratigraphic sequences: Late Jurassic, Statfjord East area, northern North Sea. Bull. Am. Ass. Petrol. Geol., 84, 45–64.

DOUGLAS, J.G. & FERGUSON, J.A. (1988) Geological Map of Victoria.

FINLAYSON, D.M., JOHNSTONE, D.W., OWEN, A.J. & WAKE-DYSTER, K.D. (1996) Deep seismic images and the tectonic framework of early rifting in the Otway Basin, Australian southern margin. Tectonophysics, 264, 1–4, 137–152.

FINLAYSON, D.M., COLLINS, C. D.N., LUKASZYK, I. & CHUDYK, E.C. (1998) A transect across Australia's southern margin in the Otway Basin region: crustal architecture and the nature of rifting from wide-angle seismic profiling. Tectonophysics, 288, 1–4, 177–189.

FOSSEN, H. & HESTHAMMER, J. (1997) Geometric analysis and scaling relations of deformation bands in porous sandstone. Journal of Structural Geology, 19, 1479-1493.
GUREVICH, B., PEVZNER, R., UROSEVIC, M., KEPIC, A., SHULAKOVA, A. & CASPARI, E. (2014) 2D and 3D seismic investigations for Stages 1 and 2C. In: Cook, P. J. (ed.): Geologically Storing Carbon: Learning from the Otway Project Experience, CSIRO Publishing, Melbourne, pp. 155–195.
HANCOCK, P.L. & BARKA, A.A. (1987) Kinematic indicators on active normal faults in western Turkey. Journal of Structural Geology, 9, 573–584.
HILLIS, R.R. & REYNOLDS, S. (2000) The Australian Stress Map. Journal of the Geological Society of London, 157, 915–921.
IMBER, J., TUCKWELL, G.W., CHILDS, C., WALSH, J.J., MANZOCCHI, T., HEATH, A.E., BONSON, C.G. & STRAND, J. (2004) Three dimensional distinct element modelling of relay growth and breaching along normal faults. Journal of Structural Geology, 26, 1897-1911.
JENKINS, C.R., COOK, P.J., ENNIS-KING, J., UNDERSHULTZ, J., BOREHAM, C., DANCE, T., DE CARITAT, P., ETHERIDGE, D.M., FREIFELD, B.M., HORTLE, A., KIRSTE, D., PATERSON, L., PEVZNER, R., SCHACHT, U., SHARMA, S., STALKER, L. & UROSEVIC, M. (2011) Safe storage and effective monitoring of CO2 in depleted gas fields. Proceedings of the National Academy of Sciences, 109, 2, E35–E41.
JONES, R.M., BOULT, P.J., HILLIS, R.R. & MILDREN, S. (2000) Integrated hydro- carbon seal evaluation in the Penola Trough, Otway Basin. The APPEA Journal, 40, 194–212.
KLEY, J., ROSSELLO, E.A., MONALDI, C.R. & HABIGHORST, B. (2005) Seismic and field evidence for selective inversion of Cretaceous normal faults, Salta rift, northwest Argentina. Tectonophysics, 399, 155–172.
KOPSEN, E. & SCHOLEFIELD, T. (1990) Prospectivity of the Otway Supergroup in the central and western Otway Basin. The APPEA Journal, 263–279.
KRASSAY, A.A., CATHRO, D.L. & RYAN, D.J. (2004) A regional tectonostratigraphic framework for the Otway Basin. Petroleum Exploration Society of Australia, Special Publication, 97–116.
KRAWCZYK, C.M., HENK, A., TANNER, D.C., TRAPPE, H., ZIESCH, J., BEILECKE, T., ARUFFO, C.M., WEBER, B., LIPPMANN, A., GOERKE, U.-J., BILKE, L. & KOLDITZ, O. (2015) Seismic and sub-seismic deformation prediction in the context of geological carbon trapping and storage. - In: Advanced Technologies in Earth Sciences, Springer, Switzerland, ISBN 978-3-319-13929-6, p. 97-113, doi: 10.1007/978-3-319-13930-2_5.
LAVIN, C.J. (1998) Geology and prospectivity of the western Victorian Voluta Trough, Otway Basin, for the 1998 Acreage Release.
LINDSAY, N. G., MURPHY, F.C., WALSH, J.J., & Watterson,J. (1993) Outcrop studies of shale smear on fault surfaces: International Association of Sedimentologists Special Publication 15, p. 113–123.
LIPPMANN, A., ENDRES, H., GIERSE, G., PRUESSMANN, J., SCHLUETER, P., EISENBERG-KLEIN, G., ZEHNDER, M., TRAPPE, H. & PROTECT RESEARCH GROUP (2013) Fracture and fault mapping by curvature and coherency analysis. Poster, CO2CRC Research Symposium, Hobart/Tasmania, 19.
LOHR, T., KRAWCZYK, C.M., ONCKEN, O. & TANNER, D.C. (2008) Evolution of a fault surface from 3D attribute analysis and displacement measurements. Journal of Structural Geology, 30, 6, 690–700.
LONG, J.J. & IMBER, J. (2012) Strain compatibility and fault linkage in relay zones on normal faults. Journal of Structural Geology, 36, 16-26.
MALLET, J.-L. (1992) Discrete smooth interpolation in geometric modelling. Computer-Aided Design, 24, 4, 178–191.
MALLET, J.-L. (2002) Geomodeling. Applied Geostatistics Series, Oxford University Press, USA.
MANSFIELD, C.S. & CARTWRIGHT, J.A. (2001) Fault growth by linkage: observations and implications from analogue models. Journal of Structural Geology, 23, 5, 745–763.
MCLEOD, A.E.N., DAWERS, H. & UNDERHILL, J.R. (2000) The propagation and linkage of normal faults: insights from the Strathspey-Brent-Statfjord fault array, northern North Sea. Basin Research, 12, 263–284.
MIDLAND VALLEY EXPLORATION LTD. (2013) Move 2013.1 Software Suite, Glasgow, U.K.
MILLER, J., NORVICK, M.S. & WILSON, C.J.L. (2002) Basement controls on rifting and the associated formation of ocean transform faults — Cretaceous continental extension of the southern margin of Australia. Tectonophysics, 359, 1–2, 131–155.
MOORE, A.M.G., STAGG, H.M.J. & NORVICK, M.S. (2000) Deep water Otway Basin: A new assessment of the tectonics and hydrocarbon prospectivity. APPEA Journal, 32, 0/1, 313–324.
MORLEY, C.K. (2002) A tectonic model for the Tertiary evolution of strike-slip faults and rift basins in SE Asia. Tectonophysics, 347, 189–215.
NEEDHAM, T., YIELDING, G. & FREEMAN, B. (1980) The tectonic evolution of the South China Sea Basin. In: Hayes, D.E. (ed): The Tectonic and Geologic Evolution of Southeast Asian Seas and Islands, Geophysical Monograph Series, 23, 89–104.
NEEDHAM, D.T., YIELDING, G. & FOX R.J. (1996a) Fault population description and prediction using examples from the offshore U.K. Journal Structural Geology, 18, 155–167.
NEEDHAM, T., YIELDING, G. & FREEMAN, B. (1996b) Analysis of fault geometry and displacement patterns. In: Buchanan, P.G. & Nieuwland, D.A. (eds): Modern Developments in Structural Interpretation, Validation and Modelling, Geological Society Special Publication, 99, 189–199.
NICOL, A., WALSH, J., BERRYMAN, K. & NODDER, S. (2005) Growth of a normal fault by the accumulation of slip over millions of years. Journal of Structural Geology, 27, 327–342.
NIXON, C.W., SANDERSON, D.J., DEE, S.J., BULL, J.M., HUMPHREYS, R.J. & SWANSON, M.H. (2014) Fault interactions and reactivation within a normal-fault network at Milne Point, Alaska. AAPG Bulletin, 98, 10, 2081-2107.

NORVICK, M. & SMITH, M.A. (2001) Mapping the plate tectonic reconstructions of southern and southeastern Australia and implications for petroleum system. The APPEA Journal, 41, 15–35.
PARADIGM LTD. (2009) Gocad 2009.3 Software Suite, Nancy, France.
PEACOCK, D.C.P. (1991) Displacements and segment linkage in strike-slip fault zones. Journal of Structural Geology, 13, 9, 1025-1035.
PEACOCK, D.C.P. & SANDERSON, D.J. (1994) Geometry and development of relay ramps in normal fault systems. AAPG Bulletin, 78, 2, 147–165.
PERINCEK, D. & COCKSHELL, C.D. (1995) The Otway Basin: Early Cretaceous rifting to Neogene inversion. Aust. Pet. Explorer Assoc. J., 35, 451–466.
PEVZNER, R., UROSEVIC, M., CASPARI, E., GALVIN, R.J., MADADI, M., DANCE, T., SHULAKOVA, V., GUREVICH, B., TCHVERDA, V. & YILDIRAY, C. (2013) Feasibility of time-lapse seismic methodology for monitoring the injection of small quantities of CO2 into a saline formation, CO2CRC Otway Project. Energy Procedia, 37, 4336–4343.
RESOR, P.G. AND MEER, V.E. (2009) Slip heterogeneity on a corrugated fault. Earth and Planetary Science Letters, 288, 3–4, 483–491.
SHARM A, S., COOK, P.J., JENKINS, C., STEEPER, T., LEES, M. & RANASINGHE, N. (2011) The CO2CRC Otway Project: Leveraging experience and exploiting new opportunities at Australia's first CCS project site. 10th International Conference on Greenhouse Gas Control Technologies. Energy Procedia, 4, 0, 5447–5454.
TUPPER, N.P., PADLEY, D., LOVIBOND, R., DUCKETT, A.K. & MCKIRDY, D.M. (1993) A key test of Otway Basin Potential: the Eumeralla-sourced play on the Charma Terrace. The APPEA Journal, 33 1, 77–93.
TVEDT, A.B.M., ROTEVATN, A., JACKSON, C.A.-L., FOSSEN, H. & GAWTHORPE, R.L. (2013) Growth of normal faults in multilayer sequences: A 3D seismic case study from the Egersund Basin, Norwegian North Sea. Journal of Structural Geology, 55, 0, 1–20.
UROSEVIC, M., PEVZNER, R., SHULAKOVA, V., KEPIC, A., CASPARI, E. & S. SHARMA (2011) Seismic monitoring of CO2 injection into a depleted gas reservoir- Otway Basin Pilot Project, Australia. Energy Procedia, 4 0, 3550–3557.
VAN RUTH, P., TENTHOREY, E. & VIDAL-GILBERT, S. (2007) Geochmechnical Analysis of the Naylor Structure, Otway Basin, Australia. Technical report.
VIDAL-GILBERT, S., TENTHOREY, E., DEWHURST, D., ENNIS-KING, J., VAN RUTH, P. & HILLIS, R. (2010) Geomechanical analysis of the Naylor Field, Otway Basin, Australia: Implications for CO2 injection and storage. International Journal of Greenhouse Gas Control, 4, 5, 827–839.
VON WINTERFELD, C. & ONCKEN, O. (1995) Non-plane strain in section balancing:
calculation of restoration parameters. Journal of Structural Geology, 17, 3, 447–450.
WALSH, J.J., BAILEY, W.R., CHILDS, C., NICOL, A. & BONSON, C.G. (2003) Formation of segmented normal faults: a 3-D perspective. Journal of Structural Geology, 25, 8, 1251–1262.
WALSH, J.J. & WATTERSON, J. (1989) Displacement gradients on fault surfaces. Journal of Structural Geology, 11, 3, 307–316.
WALSH, J.J., WATTERSON, J., BAILEY, W.R. & CHILDS, C. (1999) Fault relays, bends and branch-lines. Journal of Structural Geology, 21, 1019-1026.
WHITE, N.J., JACKSON, J.A. & McKENZIE, D.P. (1986) The relationship between geometry of normal faults and that of the sedimentary layers in their hanging walls. Journal of Structural Geology, 8, 8, 897–909.
WILLIAMSON, P.E., SWIFT, M.G., O'BRIEN, G.W. & FALVEY, D.A. (1990) Two- stage Early Cretaceous rifting of the Otway Basin margin of southeastern Australia: Implications for rifting of the Australian southern margin. Geology, 18, 1, 75–78.
WOODWARD, N.B., GRAY, D.R. & SPEAR, D.B. (1986) Including strain data in balanced cross-sections. Journal of Structural Geology, 8, 3–4, 313–324.
YIELDING, G., FREEMAN, B. & NEEDHAM, D.T. (1997) Quantitative Fault Seal Prediction. AAPG Bulletin, 81, 6, 897–917.